Journal of Alloys and Compounds 509 (2011) 4588–4594

Contents lists available at ScienceDirect

Journal of Alloys and Compounds

journal homepage: www.elsevier.com/locate/jallcom

Thermoelectric properties of $Cu_{1-x}Pt_xFeO_2$ ($0.0 \leq x \leq 0.05$) delafossite-type transition oxide

Chesta Ruttanapun[a,*], Aree Wichainchai[a], Wutthisak Prachamon[b], Anucha Yangthaisong[b], Anek Charoenphakdee[c], Tosawat Seetawan[d]

[a] Department of Applied Physics, Faculty of Science, King Mongkut's Institute of Technology Ladkrabang, Chalongkrung Road, Ladgrabang, Bangkok 10520, Thailand
[b] Department of Physics, Faculty of Science, Ubon Ratchathani University, Ubon Ratchathani 34190, Thailand
[c] Thermoelectrics and Nano Technology Research Center, Faculty of Science and Technology, Rajamangala University of Technology Suvarnabhumi, 60 Moo 3, Asian Highway, Huntra Phranakhon Si Ayutthaya 13000, Thailand
[d] Thermoelectrics Research Center and Program of Physics, Faculty of Science and Technology, Sakon Nakhon Rajabhat University 680 Nittayo Rd., Sakon Nakhon 47000, Thailand

ARTICLE INFO

Article history:
Received 16 November 2010
Received in revised form 18 January 2011
Accepted 18 January 2011
Available online 25 January 2011

Keywords:
Copper iron oxide
$Cu_{1-x}Pt_xFeO_2$
Delafossite
Thermoelectric properties
Melting point
Activation energy
Dimensionless figure of merit

ABSTRACT

The samples of $Cu_{1-x}Pt_xFeO_2$ ($0 \leq x \leq 0.05$) delafossite were synthesized by solid state reaction method for studying thermoelectric properties. The properties of Seebeck coefficient, electrical conductivity and thermal conductivity were measured in the high temperature ranging from 300 to 960 K. The results of Seebeck coefficient, electrical conductivity and power factor were increased with increasing Pt substitution and temperature. The thermal conductivity was decreased from 5.8 to 3.5 W/mK with increasing the temperature from 300 to 960 K. An important results, the highest value of power factor and ZT is 2.0×10^{-4} W/mK^2 and 0.05, respectively, for $x = 0.05$ at 960 K.

1. Introduction

Today, thermoelectric materials [1–3] have been displayed their potential as alternative sources of energy. The thermoelectric effect refers to a phenomenon whereby a gradient of temperature is converted directly into electrical current and vise versa. Furthermore, thermoelectric generators can be used to converting waste heat to produced by various sources to electrical power. The reverse effect can be practiced in thermoelectric coolers of refrigerators and other cooling systems. These conversion mechanisms have advantages of not having moving parts. The performance of the thermoelectric material is determined by the dimensionless figure of merit, $ZT = \sigma S^2 T/\kappa$, where T is the absolute temperature, S is the Seebeck coefficient, σ and κ are the electrical and thermal conductivity, respectively [3–5]. Ideally, the ZT value approaches its optimum value when σ and S are maximum, and κ is as small as possible. As the equation suggests, the efficiency increases at high temperature.

Conventional thermoelectric materials such as PbTe and Bi_2Te_3 show high values of ZT; however, they easily decompose, oxidize or melt at high temperatures in air [6]. In fact, heavy metals in Bi–Te and Pb–Te are costly and toxic [5]. This may result in a limited use in practical applications of thermoelectric power generation. Hence, the development of oxide materials with both high performance and environmentally stable at high temperature is crucial for practical applications. Recently, thermoelectric properties of oxide materials have been shown conversion efficiency close to that of conventional semimetallic materials. For example, thermoelectric voltage and direct current conductivity of transition-metal oxides such as NiO, $NaCo_2O_4$ and $Ca_3Co_4O_9$ have been reported to be large at high temperature conditions [5–8]. In addition, $CuFeO_2$ compound with delafossite structure has been reported to exhibit a large value of S (544 μV/K) and PF (0.44×10^4 W/mK^2) [9].

Delafossite compounds are classified in a group of ternary oxides whose chemical formula is $A^{+I}B^{+III}O_2$ [10,11]. Its structure is formed by alternative stacking layers of O–A–O dumbbell and BO_2 edge-shared octahedral along with the c-axis. The A^+ cation is linearly connection with O^{2-} anion in c-axis. The $[BO_2]^-$ octahedral-shaped are formed by charring of edge BO_2. The trivalent B^{3+} ions occupy in the middle of the octahedral block. The delafossite crystal has a unit cell structure of hexagonal (space group: $R3m$) and a primitive structure of rhombohedral. The A-site cations are composed of Cu, Ag, Pd, or Pt transition-metal ions maintained in a monovalent

* Corresponding author. Tel.: +66 2326 4339 53x285-6; fax: +66 2326 4413.
E-mail address: chesta.ruttanapun@gmail.com (C. Ruttanapun).

0925-8388/$ – see front matter © 2011 Elsevier B.V. All rights reserved.
doi:10.1016/j.jallcom.2011.01.113

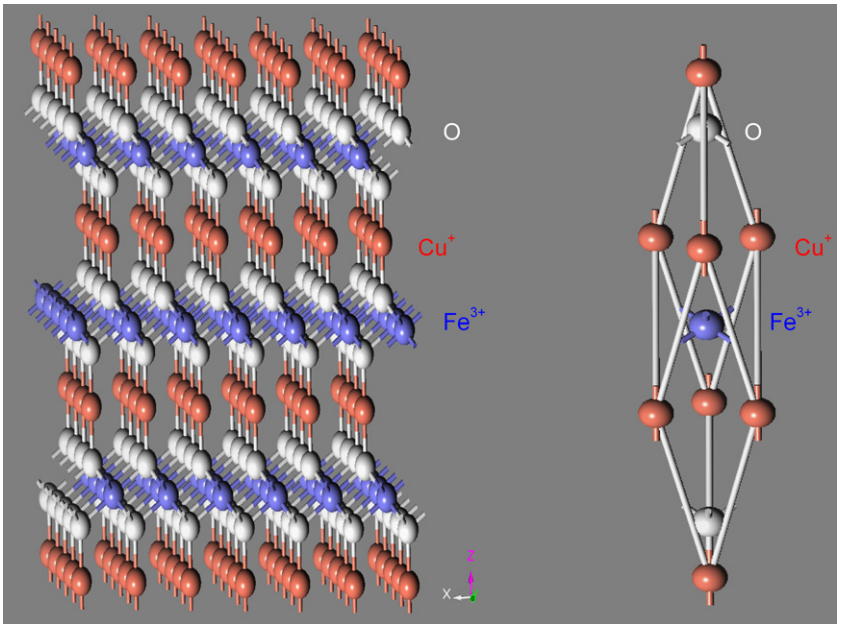

Fig. 1. The $CuFeO_2$ delafossite structure and its rhombohedral primitive cell structure.

state. The properties of delafossite are strongly dependent on which types of A-site cations being used. Cu^+ and Ag^+ (d^{10} inos) cations are responsible for semiconducting behaviors, while Pt^+ and Pd^+ (d^9 inos) cations give rise to electrical conductivity. The B-site cations mostly consist of trivalent transition metals (Cr, Mn, Fe, Co, Ni, Rh), group III metal elements (Sc, Y, La), group 13 metal elements (Al, Ga, In, Tl), or rare earths (Pr, Nd, Sm, Eu). There are many compounds in a delafossite group such as $CuFeO_2$, $CuCoO_2$, $PdCoO_2$ and $PtCoO_2$ [10–12]. The delafossite structure and rhombohedral primitive cell structure of $CuFeO_2$ are shown in Fig. 1. The Cu-based and Ag-based delafossite such as $CuFeO_2$ or $AgCoO_2$ clearly display semiconducting behavior [11,13], while the Pd-based and Pt-based delafossite such as $PdCoO_2$ or $PtCoO_2$ are metallic conductors [11,12].

Moreover, many studies have reported that $CuFeO_2$ delafossite has a *ZT* value approximately 0.04 at 960 K [14]. Other studies report that the *ZT* value of $CuFeO_2$ was improved by doping trivalent and divalent metal such as Ni, Mg Co and Ti [14–16]. However, upon doping the *ZT* was increased by less than 0.05 at 960 K. Recently, many studies have report that the Ag cations can be doped into the Cu-based delafossite such as $Cu_{1-x}Ag_xRhO_2$ [17], $Cu_{1-x}Ag_xCrO_2$ [18], and $Cu_{1-x}Ag_xAlO_2$ [19], causing the *ZT* value to improve slightly. To the best of our knowledge; however, there has been no report concerning the improvement of the *ZT* value by substituting Pt cations into Cu-base delafossite.

This paper aims to improve the *ZT* of $CuFeO_2$ delafossite by Pt substitution using solid state reaction method. The effect of partial substitution of Pt into the $CuFeO_2$ on the thermoelectric properties has been investigated. Finally, the X-ray diffraction (XRD), the Seebeck coefficient, electrical and thermal conductivity, power factor and the *ZT* value are discussed. The thermoelectric properties of the $Cu_{1-x}Pt_xFeO_2$ delafossite by partial substitution of Pt into $CuFeO_2$ in content of x for $0.0 < x < 0.05$ using solid state reaction method are reported.

2. Experimental

Bulk specimens of polycrystalline $Cu_{1-x}Pt_xFeO_2$ with $0 \le x \le 0.05$ were synthesized by a conventional direct solid-state reaction [20,21] according to the following equation:

$$2(1-x)CuO + 2(x)PtCl_2 + Fe_2O_3 \rightarrow 2Cu_{(1-x)}Pt_{(x)}FeO_2 + 2Cl_2 + (1/2)O_2.$$

Stoichiometric amounts of high-purity powders CuO (Merk, 99.98%), Fe_2O_3 (Sigma–Aldrich, Inc., 99%), and $PtCl_2$ (Sigma–Aldrich, Inc., 98%) were sufficiently mixed and ground in an agate mortar to ensure homogeneity. A homogenous mixture was obtained and cool pressed into pellets of 12 mm diameter with 2–3 mm thickness. The resulting pellets were sintered by performing on the alumina boat in furnace at 1050 °C under air atmosphere for 15–25 h. After heat treatment, the samples were rapidly quenched to room temperature. The heated pellets were repeatedly subjected to grounding, pellet, and firing procedures for several times until the pure phase of samples was obtained.

The single phase of samples was characterized by the powder X-ray diffraction (XRD) of PHILIPS model: X' Pert MPD using Cu Kα radiation with $2\theta = 10–80°$ with 0.02 steps. The lattice parameter was determined by the Rietveld refinement program, X'Pert High Score Plus V2.0a. Microstructures of the samples were observed by scanning electron microscope (SEM) using the JEOL model: JSM-5410. The decomposition analysis of the samples was analyzed using thermogravimetric method (TG) by the Pyris Diamond TG/DTG (Perkin Elmer Instrument) under air atmosphere. The electrical conductivity and Seebeck coefficient were simultaneously measured on the 4.2 mm × 2.5 mm × 20 mm sample bar using the ULVAC-RIKO ZEM-2 thermoelectric property measurement system under a low-pressure Ar atmosphere. The thermal conductivity was determined from thermal diffusivity and specific heat on pellets of 12 mm diameter with thickness of 1.6 mm by using the ULVAC SINKU RIKO Inc. model: TC-7000 laser-flash method under N_2 atmosphere. The Hall coefficient measurements were performed on the sample bar of 1 cm × 1 cm × 0.25 cm by using the Ecopai Hall measurement system model: HMS-30000 with high magnetic field strength 1.0 T at room temperature.

3. Results and discussion

3.1. Material characterization

Fig. 2 demonstrates the XRD patterns for samples of $CuFeO_2$ and the $Cu_{1-x}Pt_xFeO_2$ for $x = 0.01$, 0.03 and 0.05, respectively. The XRD peaks of the $CuFeO_2$ exhibit crystal phase of delafossite-type structure for space group: *R*3*m* corresponding to the standard ICSD: 01-075-2146 file [22] and an impurity phase of CuO related to the standard ICSD: 01-089-5897 file [22]. The others, the XRD patterns of $x = 0.01$, 0.03 and 0.05 display all peaks with relation to the peak of $CuFeO_2$.

The lattice spacing parameters of $CuFeO_2$ and $Cu_{1-x}Pt_xFeO_2$ for $x = 0.01$, 0.03 and 0.05 are shown in Fig. 3. The lattice constant of $Cu_{1-x}Pt_xFeO_2$ samples depends on the Pt in content of the *x*. The lattice distance of $CuFeO_2$ for the *a*-axis and the *c*-axis are obtained and confirmed with the finding of previous works as given 3.0334 Å and 17.1598 Å, respectively, which agrees with the standard file of

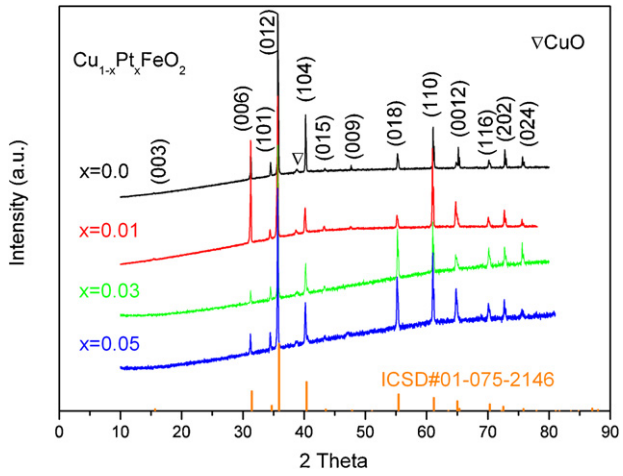

Fig. 2. The XRD patterns of the $CuFeO_2$ and the $Cu_{1-x}Pt_xFeO_2$ samples with Pt content of $x = 0.01$, 0.03 and 0.05.

ICSD: 01-075-2146 [22,23]. In addition, the $Cu_{1-x}Pt_xFeO_2$ samples, the *c*-axis rapidly increase with increasing Pt content of *x*, while the *a*-axis length still remains unchanged with increasing the *x* content. The effect of the *c*-axis increases with Pt content of *x* due to partial substitution of large ion Pt^{1+} (0.60 Å) [24] into Cu^{1+} (0.46 Å) site.

The morphology of the microstructure of $Cu_{1-x}Pt_xFeO_2$ for $x = 0.0$, 0.01, 0.03 and 0.05 samples were observed by SEM as shown in Fig. 4. The microstructure of all samples shows the giant crystal grand size (>6 μm) indicating the complete reaction in sintering process.

The decomposition of $CuFeO_2$ sample is clearly verified by thermogravimetric method (TG) in weighting loss as shown in Fig. 5. According to the entire range of measurement under the atmosphere, the first peak (368 K) is shown the effect of humidity and the second peak (495 K), oxygen is inserted approximately 0.05% into Cu layers [25–27]. The third weight loss at 556 K is originated due to oxygen excess. It is also interesting to point out that the end of the oxygen weight loss is in temperature at 980 K. Its total weight loss is approximately 0.9% which is equivalent to the oxygen content of 0.14 atoms per unit formula as indicated δ of the chemical formula $CuFeO_{(2+\delta)}$. An abrupt weight loss is observed at the temperature beyond 1365 K, indicating the melting point of the $CuFeO_2$ sample.

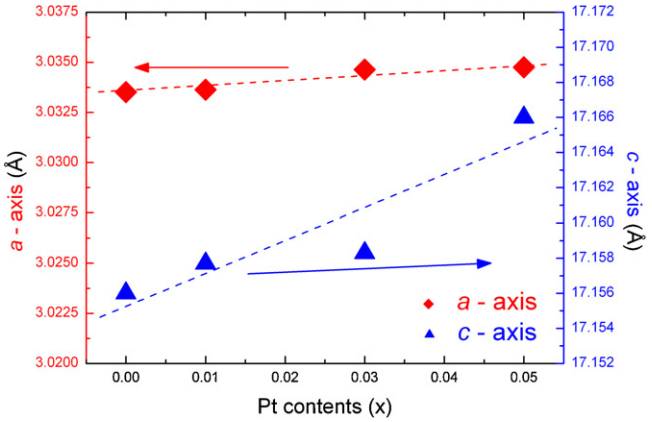

Fig. 3. The lattice parameters as a function of Pt concentration in *x* content of the $Cu_{1-x}Pt_xFeO_2$ ($0 \le x \le 0.05$) samples.

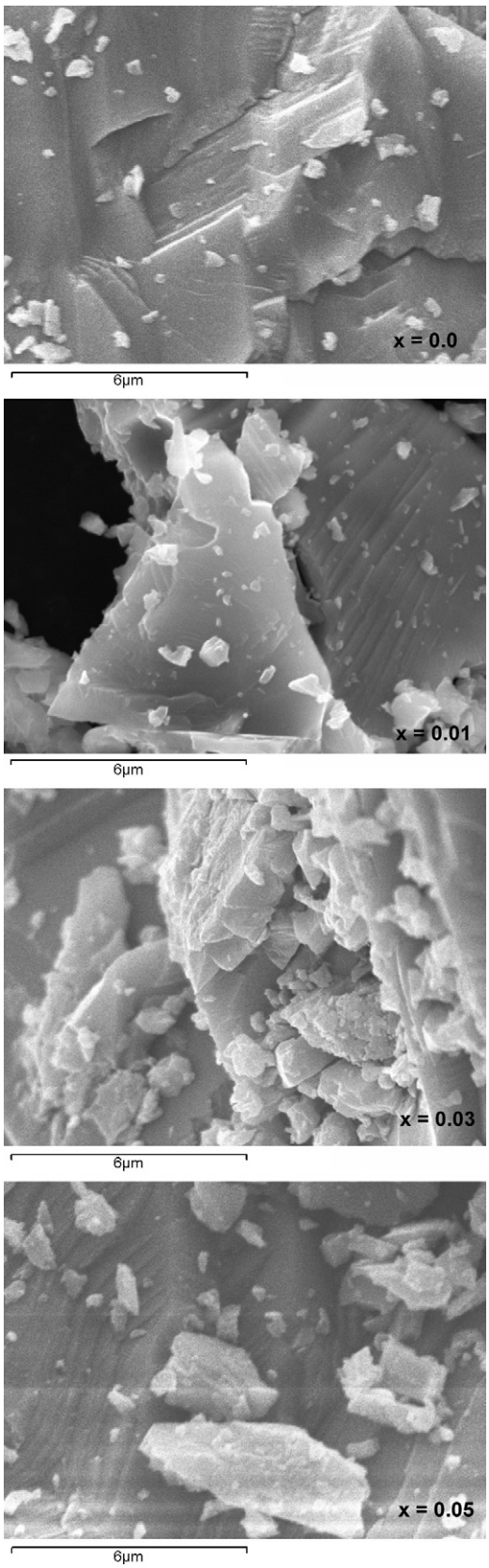

Fig. 4. The microstructure on cutting surface of the $Cu_{1-x}Pt_xFeO_2$ ($0 \le x \le 0.05$) samples.

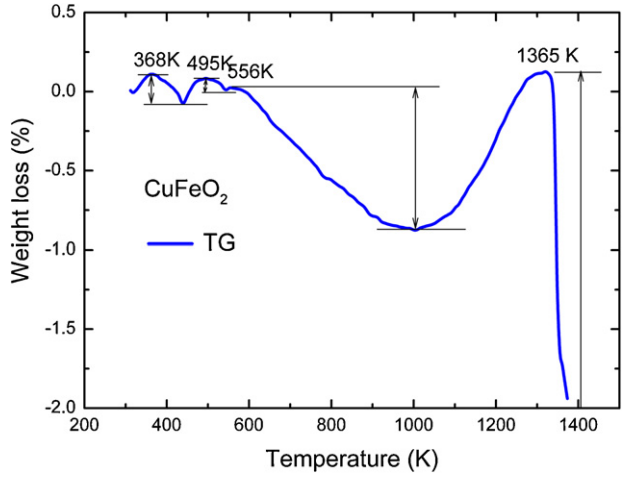

Fig. 5. The TG curve of the $CuFeO_2$ sample with temperature range from 300 to 1400 K.

3.2. Thermoelectric properties

Fig. 6(a) shows the Seebeck coefficient (S) of $Cu_{1-x}Pt_xFeO_2$ samples as a function of temperature in the range between 300 and 960 K. The results show that the Seebeck coefficients are positive sign over the measured temperature range for all samples, and they remain positive upon substitution. These results indicate that the

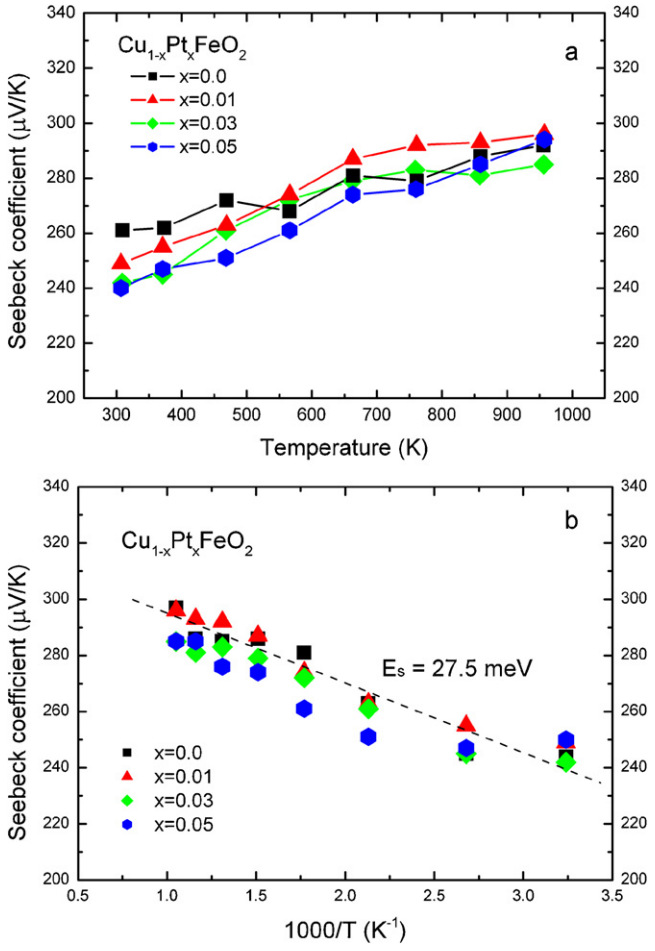

Fig. 6. (a) The Seebeck coefficient of the $Cu_{1-x}Pt_xFeO_2$ ($0 \le x \le 0.05$) samples vs. the temperature range from 300 to 960 K. (b) The curve of the Seebeck coefficient vs. $1000/T$.

$Cu_{1-x}Pt_xFeO_2$ samples with Pt substitution show p-type conductor of the thermoelectric materials. Moreover, the Seebeck coefficient of $Cu_{1-x}Pt_xFeO_2$ samples tends to increase with increasing temperature. However, the values of Seebeck coefficient decrease as a result of increased the Pt content of x. The Seebeck coefficient at 300 K is 261, 249, 242 and 240 μV/K for content of $x = 0$, 0.01, 0.03 and 0.05, respectively. The average value of the Seebeck coefficient of samples increases from 250 to 290 μV/K when the temperature increases. The maximum value of S at a high temperature (at 960 K) is 290 μV/K. This operating point might be suitable for high temperature thermoelectric devices. In addition, the results show that the Seebeck coefficient of $Cu_{1-x}Pt_xFeO_2$ samples is dependent on temperature and it decreases as a result of substitution of x content.

According to Fig. 6(a), the lowest value at 300 K for the Seebeck coefficient of $Cu_{1-x}Pt_xFeO_2$ sample for $x = 0.05$ is 240 μV/K which approximately reduces 8% comparing with the $CuFeO_2$ sample (261 μV/K). The maximum value of the reduced Seebeck coefficient of $Cu_{1-x}Pt_xFeO_2$ samples (8%) is less than the reduced value of $CuFe_{1-x}Ni_xO_2$ (26%) [14] and $CuFe_{1-x}Zn_xO_2$ (43%) [28], at temperature 300 K. This result implies that Pt^{1+} substitution in Cu^{+1} site of $CuFeO_2$ delafossite has fewer effects on the Seebeck value than the doped impurity of trivalent (such as Ni, Zn) in Fe^{3+} site of $CuFeO_2$.

In applying p-type semiconductor, the relation of the Seebeck coefficient is given by $S = (k_B/e)[(E_F - E_v)/k_BT]$ [29], where k_B is the Boltzmann's constant, e is electronic charge constant, E_v is the energy of the valance-band edge, E_F is the Fermi energy level and T is the absolute temperature. The activation energy for the production of free carriers $E_s = (E_F - E_v)$ is obtained by plotting the S vs. $1000/T$ as shown in the Fig. 6(b). The average of E_s value for all $Cu_{1-x}Pt_xFeO_2$ ($0 \le x \le 0.05$) samples is 27.5 meV. The result is slightly higher than the thermal energy at room temperature ($k_BT_{300K} \cong 25$ meV). Consequently, this value indicates that $Cu_{1-x}Pt_xFeO_2$ ($0 \le x \le 0.05$) samples are good semiconductor materials which are shallow acceptor doping level for thermoelectric devices because the charge carriers are ionized near the room temperature for conduction mechanism.

The electrical conductivity (σ) of $Cu_{1-x}Pt_xFeO_2$ samples as a function of temperature in the range of 300–960 K is shown in Fig. 7(a). The electrical conductivity of all samples is rapidly raised along with the increasing temperature and the increasing x content of Pt substitution. The values of σ at 300 K for content of $x = 0$, 0.01, 0.03 and 0.05 are 3.5, 5.0, 8.0 and 11.0 S/cm, respectively. For the sample of $x = 0.05$ at room temperature, the σ (11.0 S/cm) value is approximate four times larger than that of the $CuFeO_2$ sample (3.5 S/cm). For a high temperature at 960 K, the values ofσ are 12.5, 16.5, 19 and 23 S/cm for $x = 0.0$, 0.01, 0.03 and 0.05 respectively. The maximum value of the σ is 23 S/cm for $x = 0.05$ at a temperature of 960 K which points out that $CuFeO_2$ substitution by the Pt is suitable to use at high temperature for thermoelectric power devices. Fig. 7(b) shows the Arrhenius plot of $Cu_{1-x}Pt_xFeO_2$ ($0 \le x \le 0.05$) samples plotted by $\log\sigma$ vs. $1000/T$ in temperature ranging from 300 to 960 K. The Arrhenius plot corresponds to temperature dependence in equation $\sigma = A\exp(-E_\sigma/k_BT)$ [29], where k_B is the Boltzmann's constant, E_σ is the activation energy of conduction and A is a constant value. The activation energies (E_σ) in the Arrhenius plot, $\log\sigma$ vs. $1000/T$ are 49, 46, 33 and 28 meV for samples with x content = 0.0, 0.01, 0.03 and 0.05, respectively. These results show that the tendency of the activation energy (E_σ) decreases with increased the x content as the behavior of semiconducting of transition oxide. Fig. 7(c) shows the results of the activation energy reduces with increased Pt substitution of x content. These results exhibit that the E_σ tends to fall to zero as the substitution of x content reduces to 0.15, when metallic conduction occurs. Fig. 7(d) shows the plot of Mott's model for $Cu_{1-x}Pt_xFeO_2$ ($0 \le x \le 0.05$) samples with plotting temperature dependence in equation $\sigma = B\exp[-(T_o/T)^{1/4}]$ [29] where B and T_o are constant

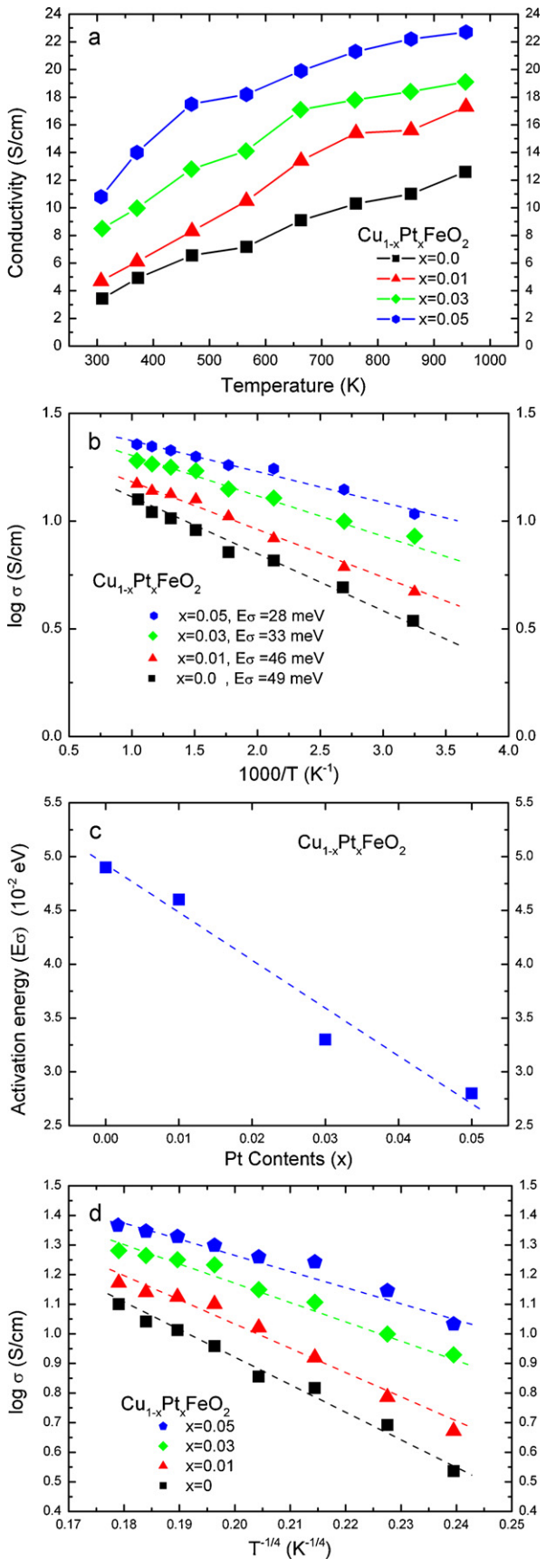

Fig. 7. (a) The electrical conductivity vs. the temperature range from 300 to 960 K. (b) The curve of log σ vs. 1000/T (c) The activation energy (E_σ) as a function of the Pt substitution in x content. (d) The curves of log σ vs. $1/T^{1/4}$.

value. The zero slope of the Mott equation implies the temperature independence of conduction which exhibits metallic behavior. The plotted results of log σ vs. $1/T^{1/4}$ in Fig. 7(d) display that $x = 0.05$ which is close to zero slope. This confirms that $Cu_{1-x}Pt_xFeO_2$ sample for $x = 0.05$ is a good semiconductor. In addition, the linear slope of log σ vs. $1/T^{1/4}$ in Fig. 7(d) suggests that a variable-range-hopping mechanism is reasonable for all samples of $Cu_{1-x}Pt_xFeO_2$ delafossite.

According to Fig. 7, the maximum conductivity value at 300 K is 11 S/cm for $x = 0.05$ of $Cu_{1-x}Pt_xFeO_2$ sample, approximately 4 times higher than the $CuFeO_2$ sample (3 S/cm). It is interesting to point out that the highest conductivity (11 S/cm) of the $Cu_{1-x}Pt_xFeO_2$ ($x = 0.05$) samples at 300 K is clearly higher than the highest value of most delafossite compounds such as $Cu_{1-x}Ag_xRhO_2$ (5 S/cm) [17], $Cu_{1-x}Ag_xAlO_2$ (2 S/cm) [19], and $CuFe_{1-x}Ni_xO_2$ (8 S/cm) [29]. These results imply that Pt^{1+} substitution in the Cu^{+1} site for $CuFeO_2$ delafossite has higher effects in electrical conduction than Ag substitution in the Cu^{+1} site and the doped impurity of trivalent (such as Ni, Mn, Co) into Fe^{3+} site. The difference value of the electrical conductivity and the activation energy of $CuFeO_2$ samples between before and after substituting Pt imply that the difference transport mechanisms in $CuFeO_2$ and $Cu_{1-x}Pt_xFeO_2$ samples is a result from the Pt substitution in the Cu-site. The p-type (hole) conductivity of the $CuFeO_2$ sample is dominated by d-orbital holes in Cu^+ ($3d_9 4s_1$) with electric charge compensation of Cu^{2+} ($3d_9$). For $Cu_{1-x}Pt_xFeO_2$ samples, the number of hole carriers increases due to ionized charge from the d-orbital of Pt^+ ($5d_8 6s_1$). In summary, the increase electrical conductivity by the Pt substitution in $Cu_{1-x}Pt_xFeO_2$ samples is enhanced because the increased hole carriers are introduced into the Cu-site.

From the equation of electrical conductivity, the relation is given by $\sigma = eN\mu$ where e is the carrier charge, N is the carrier concentration, and μ is the mobility for carriers. For the electronic transport in semiconductors, the charge carriers must be excited from bound charges to free charges, and then they are moved by mobility mechanism. Consequently, the electrical conductivity of the semiconductors is expressed by $\sigma = eN_T \exp[-(E_F - E_v)/k_BT]\mu_o \exp(-E_u/k_BT)$ [29], where N_T is the effective density of states of charge carrier, and μ_o is the mobility constant. Thus, the overall activation energy for conductor (E_σ) is a combination of two components as the relation $E_\sigma = E_\mu + E_s$ [29], where E_u is the activation energy for carrier mobility. The value of E_u is obtained from the equation $\mu = D \exp(-E_\mu/k_BT)$, where μ is the mobility of carrier and D is a constant value. From the average value of E_s (27.5 meV) and the value of E_σ (49, 46, 33 and 28 meV for $x = 0.0$, 0.01, 0.03 and 0.05, respectively), the values of E_u of $Cu_{1-x}Pt_xFeO_2$ samples are 21.5, 18.5 5.5 and 0.5 meV for $x = 0.0$, 0.01, 0.03 and 0.05, respectively, which are less than the thermal energy at room temperature ($k_BT_{300K} \cong 25$ meV). The small value of E_u implies that the temperature dependence for conductivity of the $Cu_{1-x}Pt_xFeO_2$ samples is major effect from the activation energy for carrier production. Therefore, these results confirm that the p-type conduction of $Cu_{1-x}Pt_xFeO_2$ delafossite is a good semiconductor because of the ionized free carrier occurred by activation energy near the room temperature and the moving free carriers using the activation energy of mobility smaller than the thermal energy at room temperature.

For measurement of the Hall effect of $Cu_{1-x}Pt_xFeO_2$ ($0 \le x \le 0.05$) samples at room temperature, the results exhibit p-type carrier (hole) consistent with positive sign of Seebeck coefficient in Fig. 6. The hole carrier concentrations which are calculated from Hall constant (R_H) by the relation $R_H = 1/pe$ [29] are 1.56×10^{18}, 3.86×10^{18}, 8.08×10^{18} and 4.04×10^{19} cm^{-3} for $x = 0.0$, 0.01, 0.03 and 0.05, respectively as shown in Fig. 8. The concentrations of hole carries are belong to high impurity doping of semiconductor which is difficult to find out. The results show that the hole densities increase

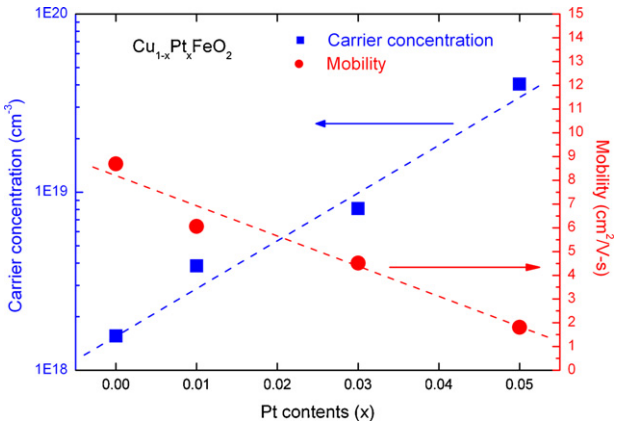

Fig. 8. The carrier concentration and mobility as a function of Pt content in x of $Cu_{1-x}Pt_xFeO_2$ ($0 \le x \le 0.05$) samples at room temperature.

with increased Pt substitution of x content. The Hall mobility (μ_H) of samples which is estimated from the relation $\sigma = pe\mu_H$ [29] are 8.6, 6.0, 4.5 and 1.8 cm^2/Vs for $x = 0.0$, 0.01, 0.03, and 0.05, respectively as shown in Fig. 8. The value of Hall mobility in the region from 1.8 to 8.6 cm^2/Vs implies that $Cu_{1-x}Pt_xFeO_2$ samples not display the behavior of small polaron because the mobility of the polaron mechanism is lowers than 0.1 cm^2/Vs [29].

Fig. 9 shows the power factor ($PF = \sigma S^2$) of $Cu_{1-x}Pt_xFeO_2$ ($0 \le x \le 0.05$) samples calculated from the measured electrical conductivity and Seebeck coefficient as function of temperature in the range of 300–960 K. The power factor of all samples is increased with increasing temperature. The power factors at 300 K for $x = 0$, 0.01, 0.03 and 0.05 are estimated to be 0.2×10^{-4}, 0.3×10^{-4}, 0.5×10^{-4} and 0.7×10^{-4} W/mK^2, respectively. The highest power factors of $Cu_{1-x}Pt_xFeO_2$ samples at 960 K are 1.1×10^{-4}, 1.5×10^{-4}, 1.7×10^{-4} and 2.0×10^{-4} W/mK^2 for $x = 0$, 0.01, 0.03 and 0.05, respectively. The maximum power factor at room temperature is 0.7×10^{-4} W/mK^2 at $x = 0.05$. The $Cu_{1-x}Pt_xFeO_2$ sample for $x = 0.05$ shows highest value of power factor reaching 2.0×10^{-4} W/mK^2 at temperature 960 K. The PF value of $Cu_{1-x}Pt_xFeO_2$ sample for $x = 0.05$ at 960 K displays 2 times and 3 times higher than the $CuFeO_2$ sample at 960 K and at 300 K, respectively. Moreover, the highest PF value of the sample for $x = 0.05$ at 960 K is higher than those reported of $CuFeO_2$ ($PF = 1.4 \times 10^{-4}$ W/mK^2) [28], $CuFe_{1-x}Ni_xO_2$ ($PF = 1.8 \times 10^{-4}$ W/mK^2) [15], and $CuAl_{1-x}Fe_xO_2$ ($PF = 0.9 \times 10^{-4}$ W/mK^2) [30].

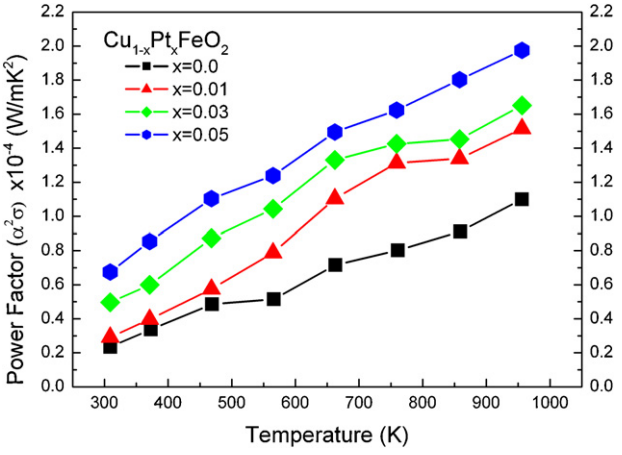

Fig. 9. The power factor of $Cu_{1-x}Pt_xFeO_2$ ($0 \le x \le 0.05$) samples vs. the temperature range of 300–960 K.

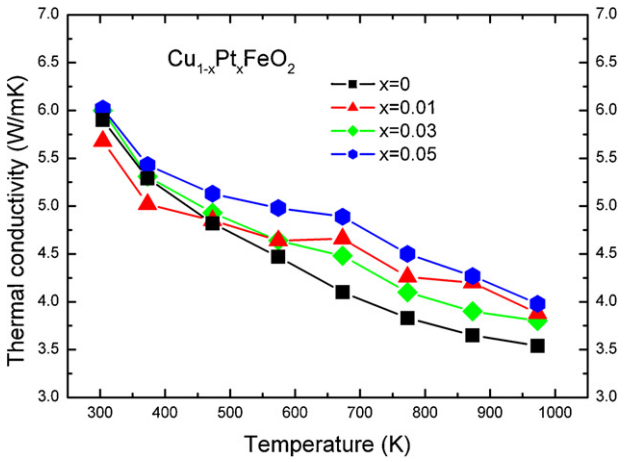

Fig. 10. The thermal conductivity of the $Cu_{1-x}Pt_xFeO_2$ ($0 \le x \le 0.05$) samples vs. the temperature range from 300 to 960 K.

The temperature dependence of thermal conductivity on $Cu_{1-x}Pt_xFeO_2$ ($0 \le x \le 0.05$) samples as function of temperature in the range from 300 to 960 K is shown in Fig. 10. The samples were measured by using a laser flash method with the relation of $\kappa = dC_pa$ [31], where d, C_p and a are the density of sample, specific heat and thermal diffusivity, respectively. The bulk density of $Cu_{1-x}Pt_xFeO_2$ samples for $x = 0$, 0.01, 0.03 and 0.05 are 5.22, 5.21, 5.20 and 5.19, respectively, as exhibited in Table 1. The ratios of bulk density to calculation density of $Cu_{1-x}Pt_xFeO_2$ samples have ranging from 91 to 96%. The results of thermal conductivity of $Cu_{1-x}Pt_xFeO_2$ samples decrease as a result of increasing temperature as shown in Fig. 10. The κ values of $Cu_{1-x}Pt_xFeO_2$ samples lead to minimal increase with increased Pt substitution x content. The κ values of $CuFeO_2$ sample are in the range from 5.8 to 3.5 W/mK with a region of temperature 300–960 K. For $Cu_{1-x}Pt_xFeO_2$ sample for $x = 0.05$, the κ value is slightly higher about 1.1 time than that value of $CuFeO_2$ sample. The minimum of κ value (3.5 W/mK) is in $CuFeO_2$ sample at high temperature 960 K. The yield of thermal conductivity exhibits that $Cu_{1-x}Pt_xFeO_2$ samples decrease with increased temperature. Therefore, the high value of Z and ZT of $Cu_{1-x}Pt_xFeO_2$ samples is dominant to occur in high temperature because the κ value still contains minimum value in high temperature.

The total thermal conductivity (κ) consists of the two components: the lattice (phonon) component and electronic component as in following the reaction $\kappa = \kappa_l + \kappa_e$ [31], where the κ_l and κ_e are the thermal conductivity of phonon and the electronic contribution, respectively. From the Wiedmann–Franz law [31], the κ_e is related by $\kappa_e = L_oT\sigma$, where L_o is the Lorenz factor (2.45×10^{-8} $W\Omega/K^2$), T is the absolute temperature, σ is the electrical conductivity. From the highest σ value (23 S/cm) of $Cu_{1-x}Pt_xFeO_2$ samples for $x = 5$ at 960 K, the κ_e value is 5.409×10^{-2} W/mK which is 1.545% of the total κ value. This result indicates that the major effect of thermal conductivity of $Cu_{1-x}Pt_xFeO_2$ samples is dominated by the phonon mechanism part.

For the lattice thermal conductivity (κ_l), The Umklapp scattering contribution in the phonon scattering process is expressed by $\kappa_u = \delta[(T_m)^{3/2}M^{(-7/6)}\rho^{2/3}]T^{(-1)}$ [32], where κ_u is the Umklapp phonon thermal conductivity, δ is the proportionality constant,

Table 1
Bulk densities of the $Cu_{1-x}Pt_xFeO_2$ ($0 \le x \le 0.05$) samples and their ratios to the theoretical density.

x	0.0	0.01	0.03	0.05
Density (g/cm^3)	5.22	5.21	5.20	5.19
Ratio (%)	96.84	95.94	94.20	91.97

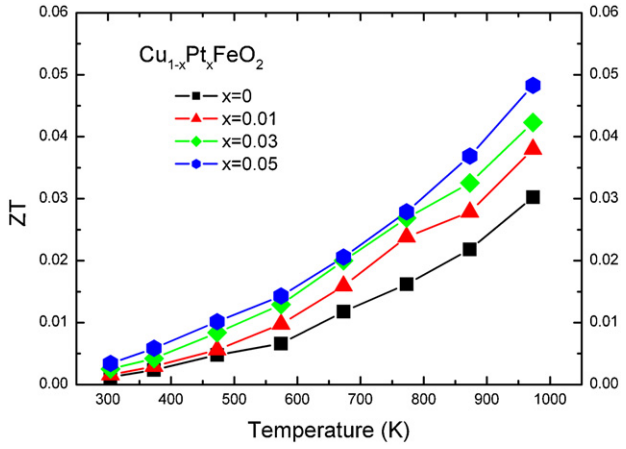

Fig. 11. The dimensionless figure of merit (ZT) of $Cu_{1-x}Pt_xFeO_2$ ($0 \le x \le 0.05$) samples vs. the temperature range from 300 to 960 K.

T_m is the melting temperature, M is the average atomic mass, ρ is the density, and T is the operation temperature. The Umklapp relation implies that the κ_u value is proportion to inversion of temperature. From Fig. 10, the thermal conductivity of $Cu_{1-x}Pt_xFeO_2$ samples can plot in function of inversion temperature as the relation of κ vs. 1000/T. The curve can show the thermal conductivity of $Cu_{1-x}Pt_xFeO_2$ samples linear with T^{-1} corresponding with the Umklapp relation. This result indicates that the major effect of thermal conductivity of $Cu_{1-x}Pt_xFeO_2$ samples is controlled by phonon mechanism with contribution by the Umklapp scattering. From the Umklapp relation, the minimum of thermal conductivity for $Cu_{1-x}Pt_xFeO_2$ samples is occurred by operating in high temperature near melting point (1365 K) temperature.

The temperature dependence of ZT for $Cu_{1-x}Pt_xFeO_2$ samples in temperature ranging from 300 to 960 K is exhibited in Fig. 11. The ZT values are also calculated from Z value and temperature. The results show that the ZT of $Cu_{1-x}Pt_xFeO_2$ samples rapidly is raised with increasing the temperature. In addition, the ZT values of $Cu_{1-x}Pt_xFeO_2$ samples are increased with increased Pt substitution of x content. The maximum ZT values of $Cu_{1-x}Pt_xFeO_2$ samples are 0.03, 0.038, 0.044 and 0.05 for $x = 0$, 0.01, 0.03 and 0.05, respectively, at 960 K. Obviously, the $Cu_{1-x}Pt_xFeO_2$ sample of $x = 0.05$ exhibits the highest value of ZT (=0.05), at 960 K. This value is higher than those reported of $CuFeO_2$ ($ZT = 0.025$) [28], $CuAlO_2$ ($ZT = 0.004$) [19], $Cu_{1-x}Ag_xAlO_2$ ($ZT = 0.016$) [30], and $CuFe_{1-x}Ni_xO_2$ ($ZT = 0.045$) [14].

4. Conclusions

The objective of this study was to improve ZT value of $CuFeO_2$ delafossite by Pt substitution in content of $x = 0.0$, 0.01, 0.03, 0.05. The samples were prepared by the conventional solid state reaction method. The results of this study show that $CuFeO_2$ sample is decomposed at temperature over 1365 K. The properties of Seebeck coefficient, electrical conductivity and thermal conductivity were measured and discussed in the high temperature ranging from 300 to 960 K. The Seebeck coefficient of all $Cu_{1-x}Pt_xFeO_2$ samples not only display the p-type semiconductor, but also show the Seebeck coefficient at 300 K in 261, 149, 242 and 240 μV/K for $x = 0$, 0.01, 003 and 0.05, respectively. It is also to point out that the average Seebeck coefficient in high temperature (at 960 K) is in the order 290 μV/K. In addition, the room temperature of the electrical conductivity increases from 3.5 to 11 S/cm with increased Pt content of x. The highest electrical conductivity is 23 S/cm for $x = 0.05$ at 960 K. Furthermore, the highest power factor is 2.0×10^{-4} W/mK^2 for $x = 0.05$ at 960 K. The thermal conductivity of $CuFeO_2$ sample decreases from 5.8 to 3.5 W/mK with increasing temperature. The minimum thermal conductivity is 3.5 W/mK of $CuFeO_2$ sample at 960 K. Most interestingly, the highest ZT is 0.05 for $x = 0.05$ at 960 K. These results suggest that the effect of small Pt substitution into $CuFeO_2$ improves the thermoelectric properties and enhances the good semiconductor behavior. In summary, the present work demonstrates that $CuFeO_2$ substituted by Pt has been given an enhanced performance on thermoelectric material. It will be interesting to see that $Cu_{1-x}Pt_xFeO_2$ delafossite material in the future can be invented the thermoelectric device for covering heat loses at high temperature.

Acknowledgments

The authors would like to thank the Department of Chemistry, Faculty of Science, Ubon Ratchathani University for providing TG–DTA facilities; the Department of Applied Physics, Faculty of Science, King Mongkut's Institute of Technology Ladkrabang (KMITL) for providing $PtCl_2$ powder. The contribution of anonymous reviewers and language editors are also acknowledged for providing valuable feedback and suggestions to improve the article.

References

[1] J. Li, W. Liu, L. Zhao, M. Zhou, NPG Asia Mater. 2 (2010) 152–158.
[2] G.J. Snyder, E.S. Toberer, Nat. Mater. 7 (2008) 105–114.
[3] A. Charoenphakdee, K. Kurosaki, A. Harnwunggmoung, H. Muta, S. Yamanaka, J. Alloy Compd. 496 (2010) 53–55.
[4] X. Hou, Y. Zhou, L. Wang, W. Zhang, W. Zhang, L. Chen, J. Alloy Compd. 482 (2009) 544–547.
[5] D. Kenfaui, D. Chateigner, M. Gomina, J.G. Noudem, J. Alloy Compd. 490 (2010) 472–479.
[6] H. Ohta, K. Sugiura, K. Koumoto, J. Inorg. Chem. 47 (2008) 8429–8436.
[7] T. Seetawan, V. Amornkitbamrung, T. Burinprakhon, S. Maensiri, P. Tongbai, K. Kurosaki, H. Muta, M. Uno, S. Yamanaka, J. Alloy Compd. 416 (2006) 291–295.
[8] S. Maensiri, W. Nuansing, Mater. Chem. Phys. 99 (2006) 104–108.
[9] T. Kajitani, T. Nozaki, K. Hayashi, Adv. Sci. Technol. 74 (2010) 66–71.
[10] M.A. Marquardt, N.A. Ashmore, D.P. Cann, Thin Solid Films 496 (2006) 146–156.
[11] M. Beekman, J. Salvador, X. Shi, G.S. Nolas, J. Yang, J. Alloy Compd. 489 (2010) 336–338.
[12] V. Eyert, R. Frésard, A. Maignan, J. Chem. Mater. 20 (2008) 2370–2373.
[13] V. Eyert, R. Frésard, A. Maignan, Phys. Rev. B 78 (2008) 052402.
[14] K. Hayashi, T. Nozaki, T. Kajitani, Jpn. J. Appl. Phys. 46 (2007) 5226–5229.
[15] T. Nozaki, K. Hayashi, T. Kajitani, J. Chem. Eng. Jpn. 40 (2007) 1205–2007.
[16] T. Nozaki, K. Hayashi, T. Kajitani, J. Electron. Mater. 39 (2010) 1798–1802.
[17] S. Shibasaki, W. Kobayashi, I. Terasaki, J. Phys. Rev. B 74 (2006) 235110.
[18] T. Okuda, T. Kishimoto, K. Uto, T. Hokazono, Y. Onose, Y. Tokura, R. Kajimoto, M. Matsuda, J. Phys. Soc. Jpn. 78 (2009) 13604.
[19] S. Yanagiya, N. Nong, J. Xu, N. Pryds, Materials 3 (2010) 318–328.
[20] A. Wichainchai, P. Dordor, J.P. Doumerc, E. Marquestaut, M. Pouchard, P. Hagenmuller, J. Solid State Chem. 74 (1988) 126.
[21] P. Dordor, J.P. Chaminade, A. Wichainchai, E. Marquestaut, J.P. Doumerc, M. Pouchard, P. Hagenmuller, A. Ammar, J. Solid State Chem. 75 (1988) 105–112.
[22] ICSD Card File: 01-075-2146, ICSD Card File:01-089-5897.
[23] T.R. Zhao, M. Hasegawa, T. Kondo, T. Yagi, H. Takei, Mater. Res. Bull. 32 (1997) 151–157.
[24] C.T. Prewitt, R.D. Shannon, D.B. Rogers, J. Inorg. Chem. 10 (1971) 719–723.
[25] B. Bellal, S. Saadi, N. Koriche, A. Bouguelia, M. Trari, J. Phys. Chem. Solids 70 (2009) 1132–1136.
[26] R.J. Cava, R.J. Cava, H.W. Zandbergen, A.P. Ramirez, H. Takagi, C.T. Chen, J.J. Krajewski, W.F. Peck Jr., J.V. Waszczak, G. Meigs, R.S. Roth, L.F. Schneemeyer, J. Solid State Chem. 104 (1993) 437–452.
[27] K. Isawa, Y. Yaegashi, M. Komatsu, M. Nagano, S. Sudo, M. Karppinen, H. Yamauchi, J. Phys. Rev. B 56 (1997) 3457–3466.
[28] T. Nozaki, K. Hayashi, T. Kajitani, 26th International Conference on Thermoelectrics, ICT 2007, 2008, pp. 167–170.
[29] P.A. Cox, Transition Metal Oxides, Clarendon Press, Oxford, 1995.
[30] K. Park, K.Y. Ko, H.-C. Kwon, S. Nahm, J. Alloy Compd. 437 (2007) 1–6.
[31] A.F. Ioffe, Infosearch limited, London, 1957.
[32] N. Schwartz, W. Tantraporn, W.J. Van Der Grinten, Advanced Energy Conversion, Pergamon Press, 1963.